Supporting Information

An efficient upconversion photocatalyst of $Er^{3+}/Tm^{3+}/Yb^{3+}$ tridoped ($CaWO_4$@(TiO_2/CaF_2)) by multi-stage CaF_2 nanocrystal formation

Shouqiang Huang, Ziyang Lou, Aidang Shan, Nanwen Zhu,* Kaili Feng and Haiping Yuan

School of Environmental Science and Engineering, Shanghai Jiao Tong University, 800 Dongchuan Road, Shanghai, 200240, P. R. China. Tel.: +86 21 54743710; Fax: +86 21 54743710. E-mail: nwzhu@sjtu.edu.cn

Table S1 The corresponding values of output currents and powers in the 980 nm semiconductor solid laser

Output Currents (A)	Output Powers (W)
1.0	0.66
1.5	1.13
2.0	1.64
2.5	2.07
3.0	2.58

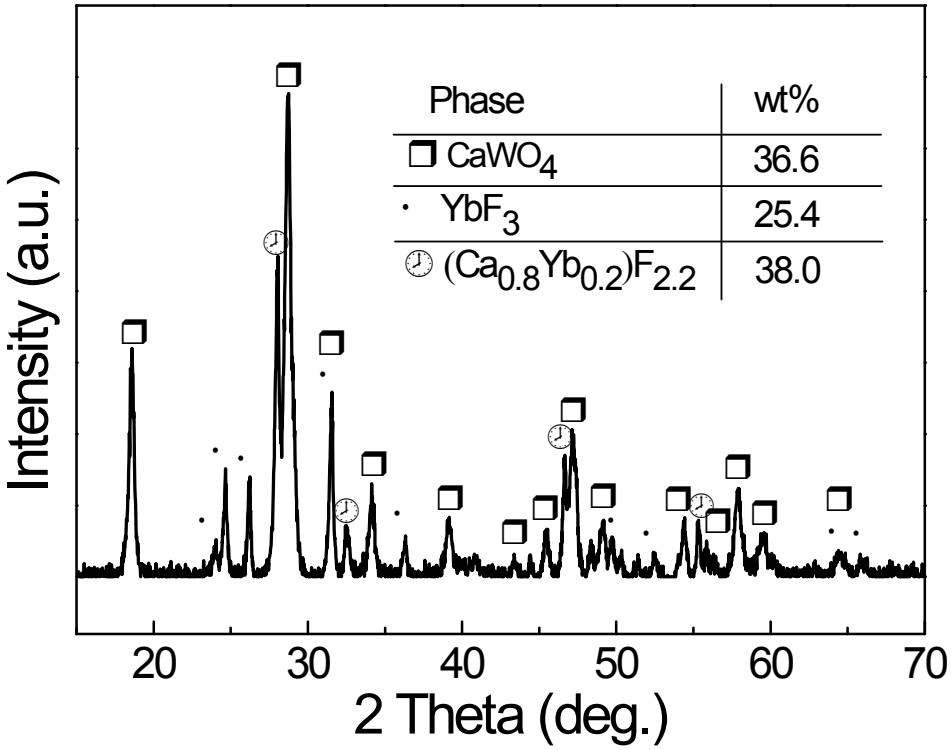

Fig. S1 XRD pattern of ETY-CC and weight fractions of each phase.

As shown in Figure S1, the main diffraction peaks at 18.62º, 28.76º, 31.53º, 34.18º, and 47.18º are assigned to the (101), (112), (004), (200), and (204) planes of $CaWO_4$ (PDF-#72-1624). The diffraction peaks at 23.98°, 24.62°, and 36.28° are indexed to the (011), (101), and (020) planes of YbF_3 (PDF-#74-2178), respectively. The phase compositions of ETY-CC are calculated by MDI's Jade software,[1] and the weight fractions of $CaWO_4$, YbF_3, and $(Ca_{0.8}Yb_{0.2})F_{2.2}$ are about 36.6%, 25.4%, and 38.0%,

respectively (Fig. S1). Usually, the phase ratio of $CaWO_4$, YbF_3, and $(Ca_{0.8}Yb_{0.2})F_{2.2}$ in the ETY-CTC system is similar to that in ETY-CC, since the introduction of TiO_2 will not affect the structure greatly under the same preparation conditions.

Table S2 Average crystal sizes and optics properties of the samples.

Samples	Average crystal sizes (nm)				BET (m^2/g)	Pore size (nm)	Band gap energy (eV)	Absorption edge (nm)
	TiO_2	$CaWO_4$	YbF_3	$(Ca_{0.8}Yb_{0.2})F_{2.2}$				
ETY-CC	-	45.69	37.23	26.04	-		-	-
ETY-CT	13.49	45.29	-	-	70	7.53	2.96	419
ETY-CTC	12.35	45.56	38.05	28.02	19	15.20	2.92	425

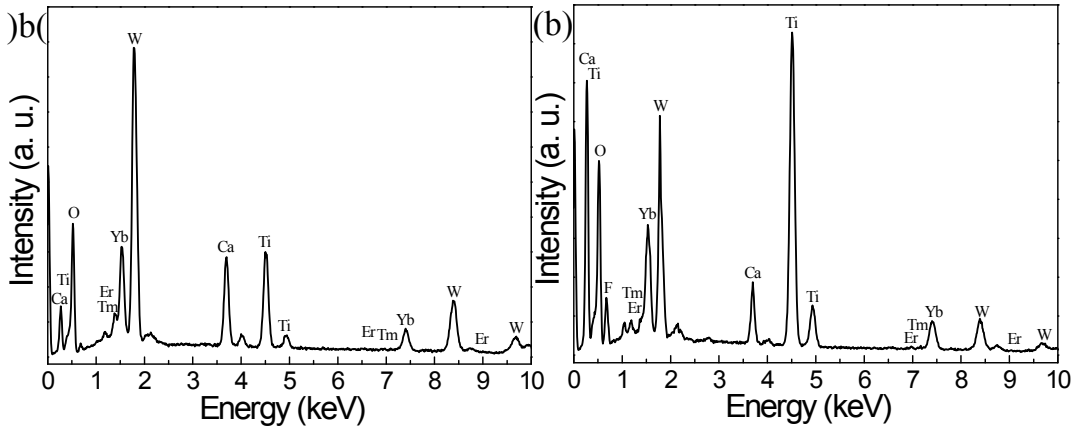

Fig. S2 EDS spectra of (a) ETY-CT and (b) ETY-CTC.

Table S3 Chemical element contents of the samples obtained from EDS and XPS.

Samples	Element contents (Atomic %) from EDS							
	Ti	Ca	Yb	Er	Tm	W	F	O
ETY-CT	10.50	8.33	3.83	0.25	0.25	10.45	-	66.38
ETY-CTC	16.08	3.88	2.27	0.17	0.20	4.01	14.46	58.92
	Element contents (Atomic % from XPS)							
ETY-CTC	Ti: Ca: F: W: Yb = 33.41: 4.06: 5.43: 9.84: 2.57 (Ca: F: W: Yb = 1: 1.34: 2.42: 0.63)							
ETY-CC	Ca: F: W: Yb = 23.30: 38.52: 6.31: 5.92 (Ca: F: W: Yb = 1: 1.65: 0.27: 0.25)							

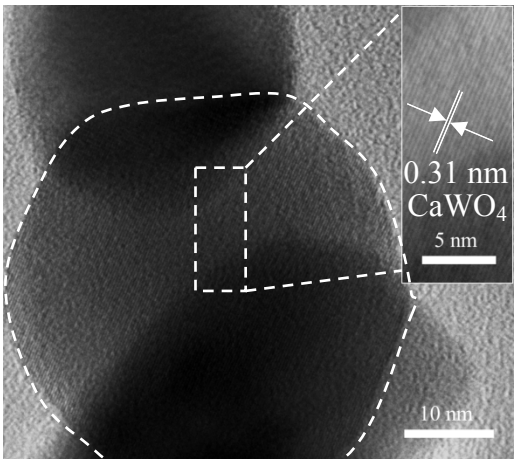

Fig. S3 HRTEM image of $CaWO_4$ nanocrystal with the size of about 45 nm, and the inset shows the lattice fringe spacing of 0.31 nm, which is closed to the (112) planes of $CaWO_4$.

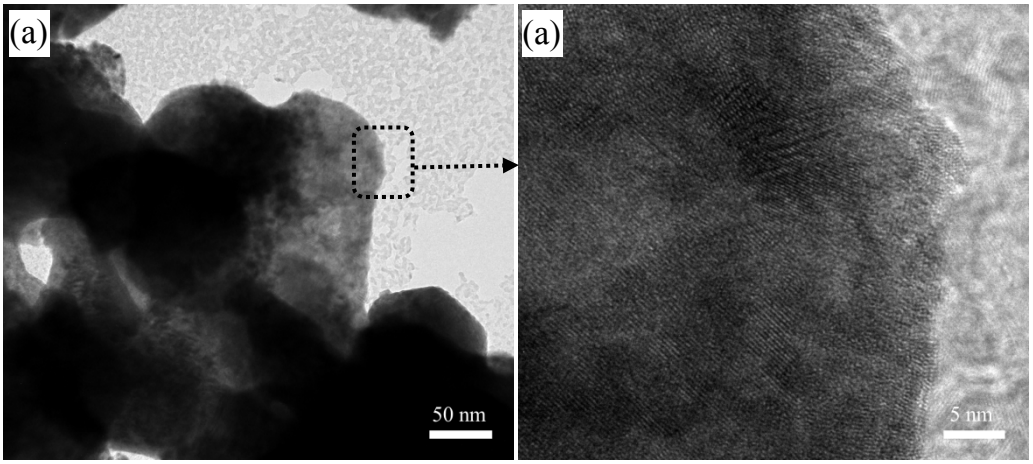

Fig. S4 (a) TEM and (b) HRTEM images of ETY-CC nanocrystals.

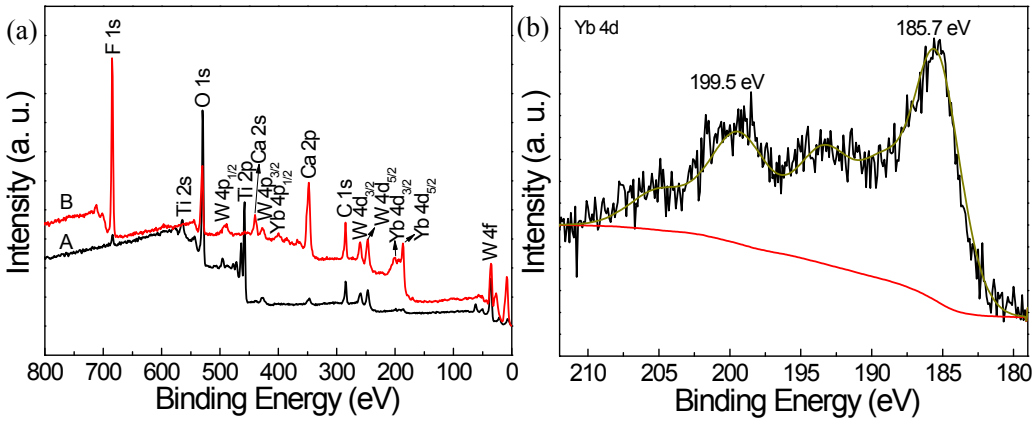

Fig. S5 (a) Survey-scan XPS spectra of (A) ETY-CTC and (B) ETY-CC. XPS spectra of ETY-CTC: (b) Yb 4d.

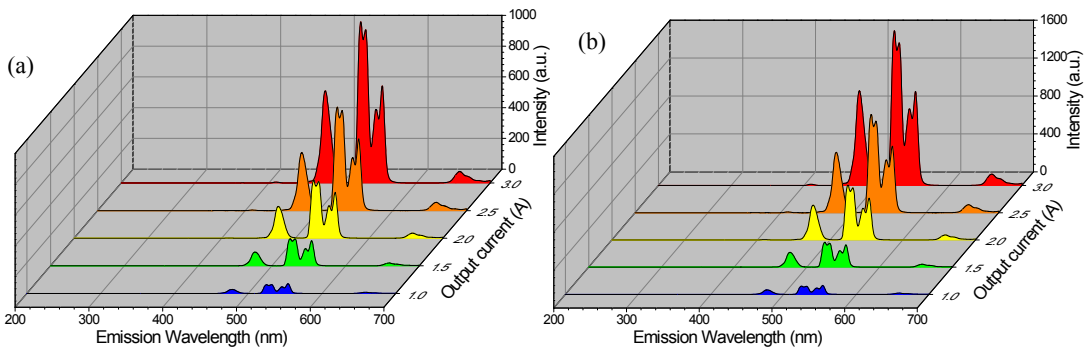

Fig. S6 Upconversion luminescence spectra of (a) ETY-CC and (b) ETY-CTC under 980 nm NIR excitation with different output currents (1.0-3.0 A).

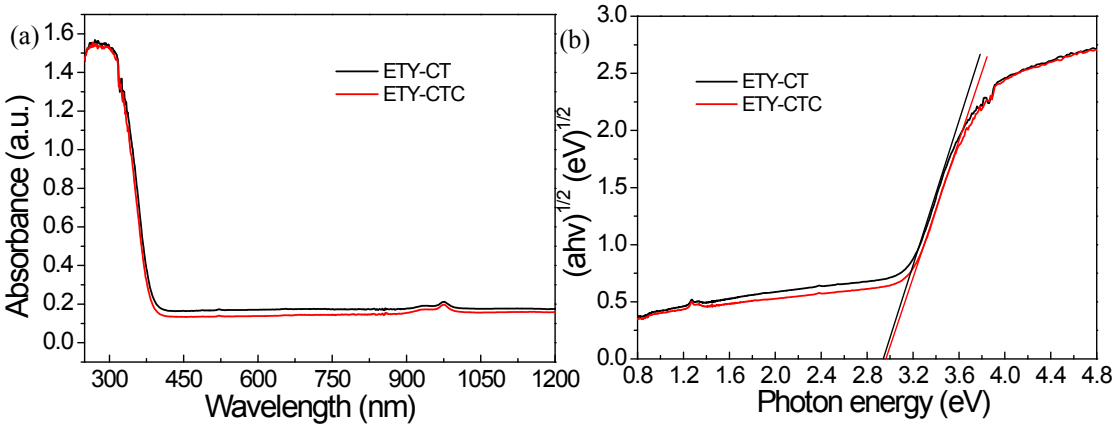

Fig. S7 (a) UV-vis-NIR diffuse reflectance spectra and (b) the plots of the $(\alpha h\nu)^{1/2}$ versus photon energy ($h\nu$) for ETY-CT and ETY-CTC. From the UV-vis-NIR absorption spectrum (Fig. S5a), the light absorption properties of ETY-CT and ETY-CTC exhibit little difference, and their band gap energies are calculated from the $(\alpha h\nu)^{1/2}$ versus photon energy ($h\nu$) plots (Fig. S5b) to be 2.96 (419 nm) and 2.92 eV (425 nm), respectively (Table S1).

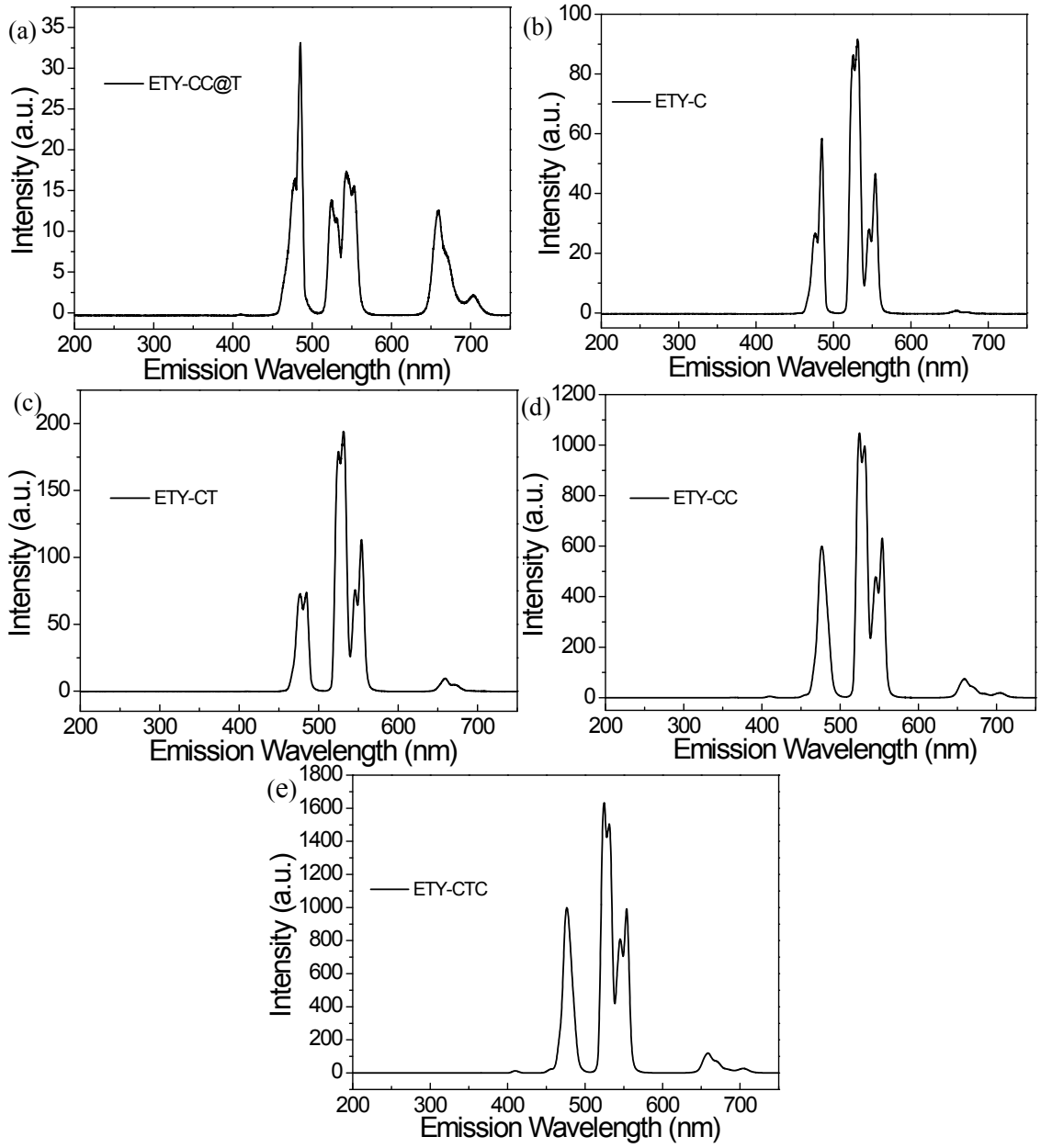

Fig. S8 Upconversion luminescence spectra of (a) ETY-CC@T, (b) ETY-C, (c) ETY-CT, (d) ETY-CC, and (e) ETY-CTC under 980 nm light excitation (output current = 3.0 A).

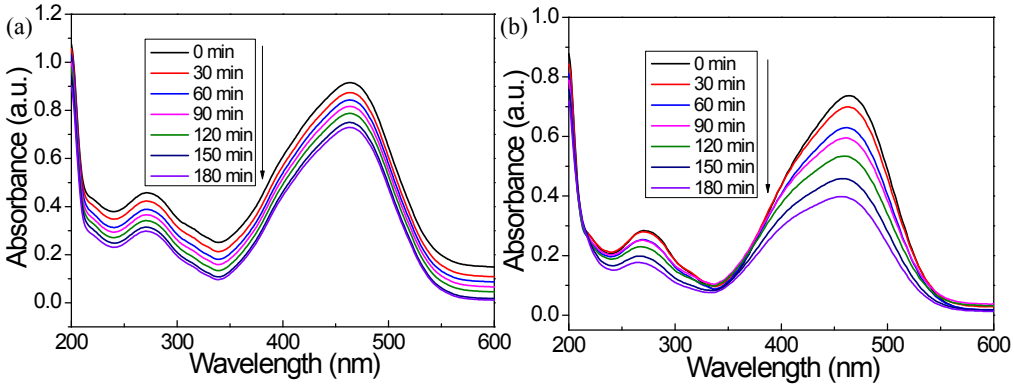

Fig. S9 Time-dependent absorption spectra of MO for ETY-CTC under (a) 980 nm (output current = 2.0 A) and (b) NIR (λ ≥ 780 nm) light (provided by high pressure mercury lamp) irradiations.

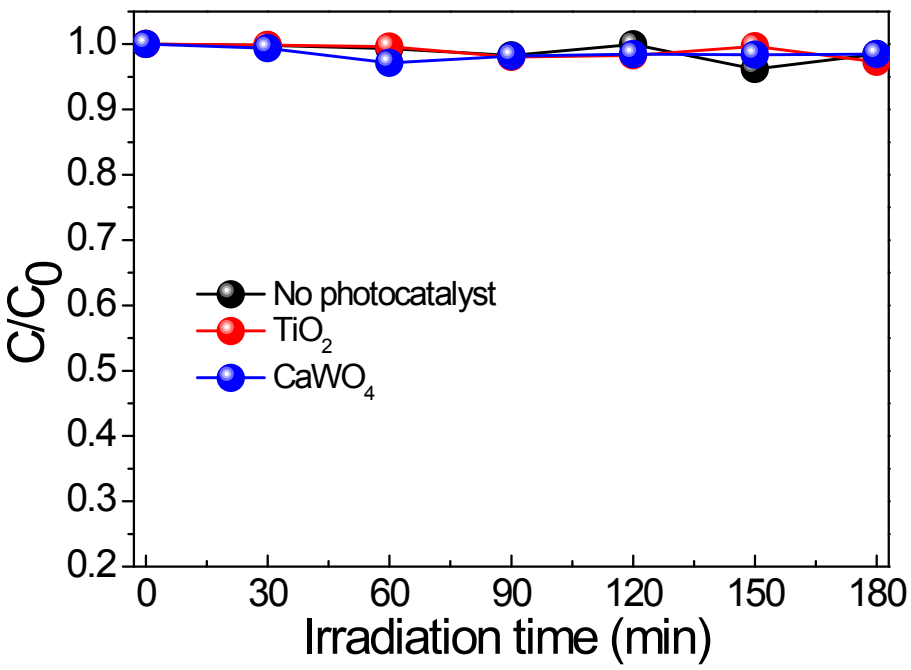

Fig. S10 C/C_0 conversion plots of MO for TiO_2 and $CaWO_4$ under NIR light (λ ≥ 780 nm) irradiation.

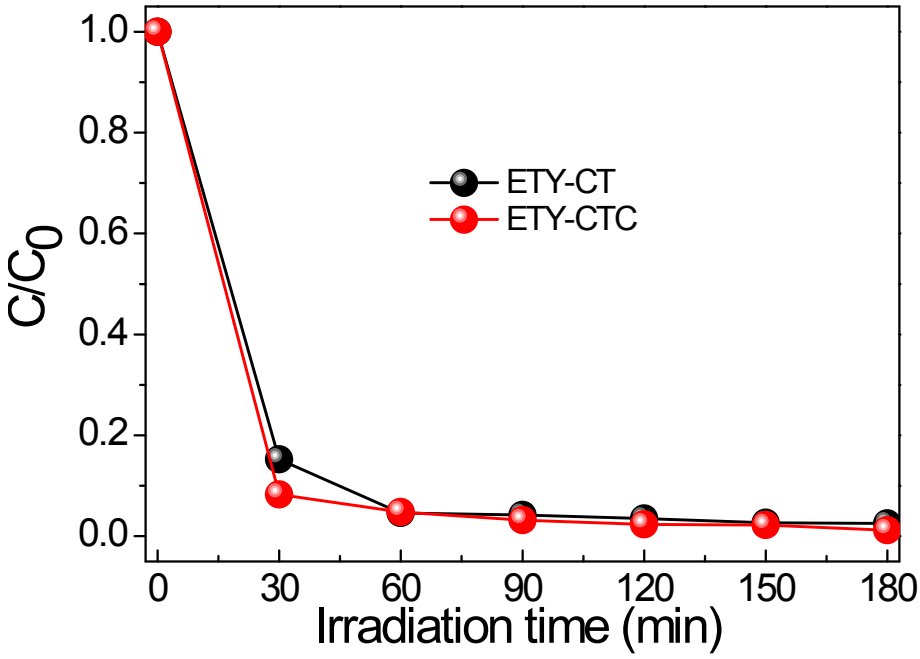

Fig. S11 C/C_0 conversion plots of MO for ETY-CT and ETY-CTC under UV-vis-NIR irradiation.

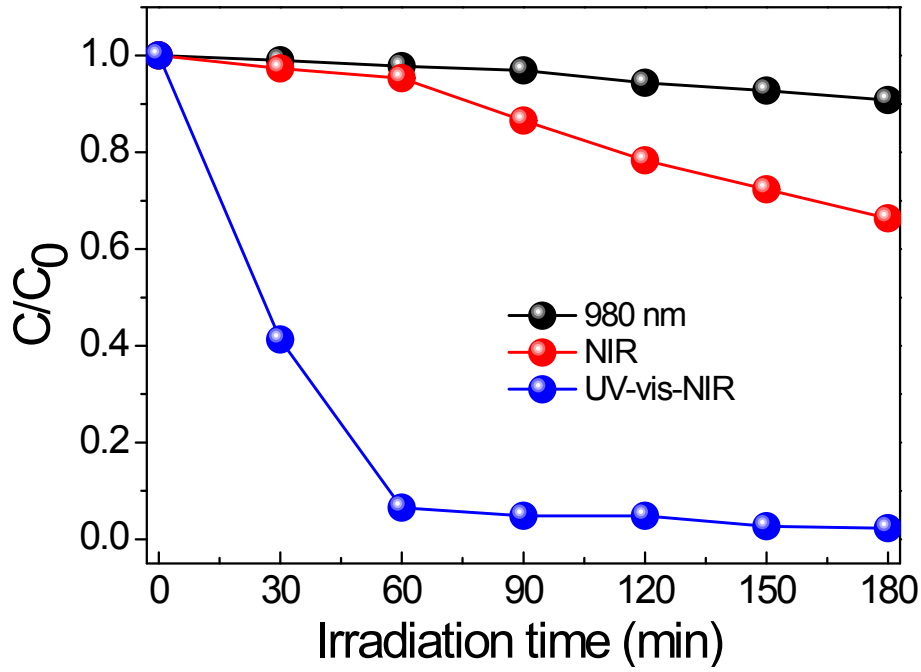

Fig. S12 C/C_0 conversion plots of MO for ETY-CC@T under 980 nm (output current = 2.0 A), NIR ($\lambda \geq 780$ nm) and UV-vis-NIR light irradiations.

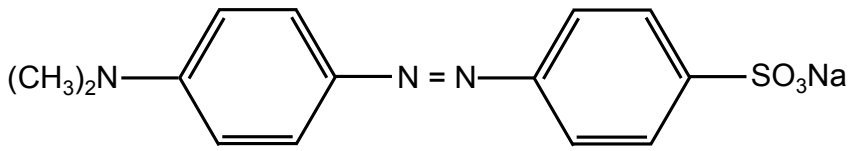

Fig. S13 Structure of MO molecule.

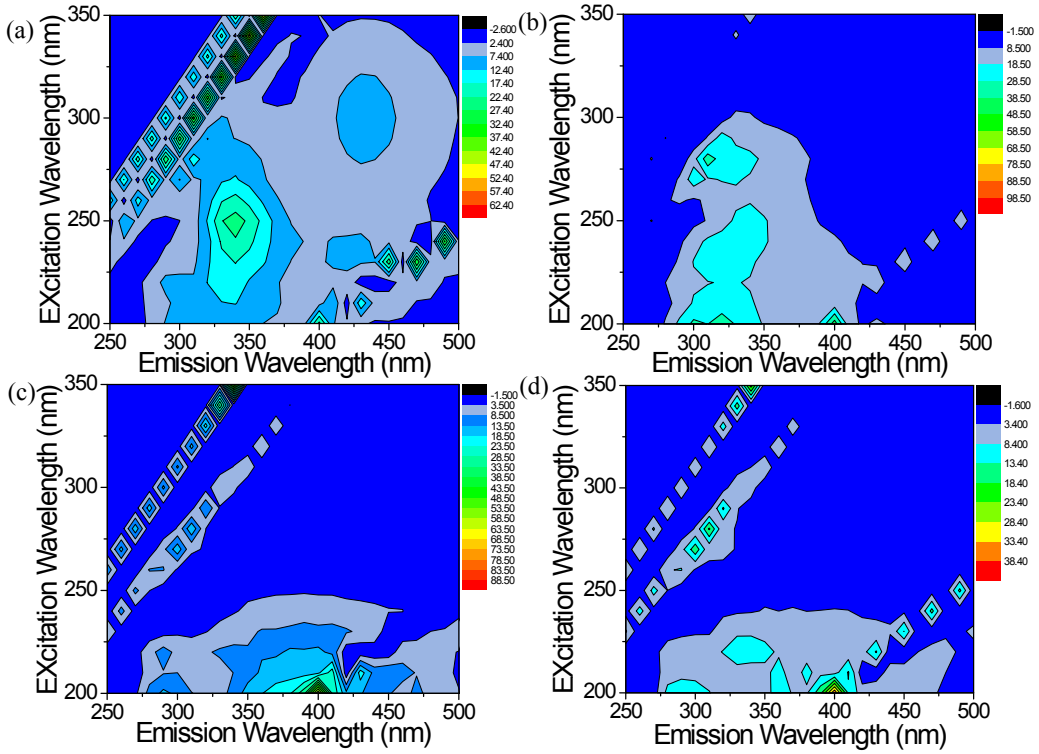

Fig. S14 EEM fluorescence spectra of MO for ETY-CTC under UV-vis-NIR irradiation: (a) 0 min, (a) 30 min, (a) 120 min, and (a) 180 min.

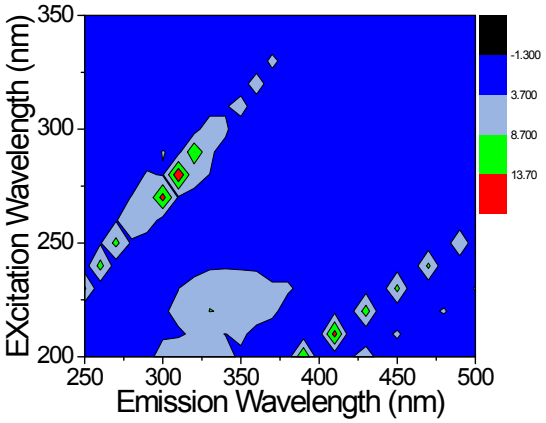

Fig. S15 EEM fluorescence spectrum of the distilled water used in this study.

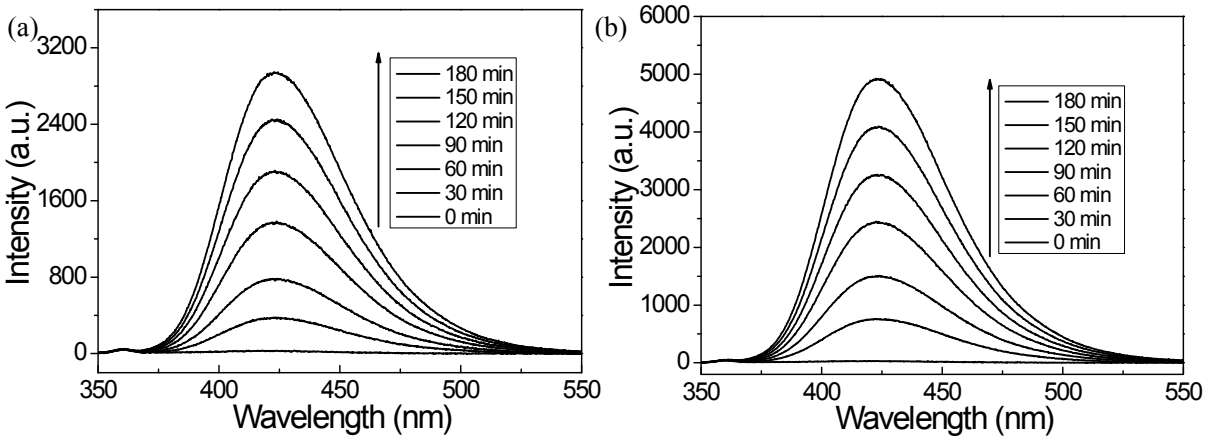

Fig. S16 Time-dependent fluorescence spectra of the terephthalic acid solution over the photocatalysts of (a) ETY-CT and (b) ETY-CTC under 980 nm light irradiation (output current = 2.0 A). The PL intensities of 2-hydroxyterephthalic acid at about 423 nm increase gradually as the irradiation time extended.

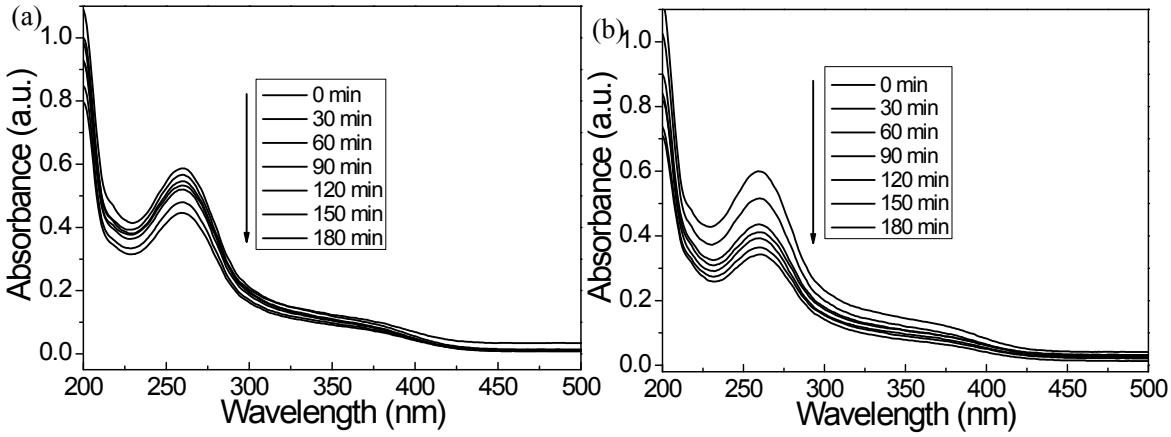

Fig. S17 Time-dependent absorption spectra of NBT for (a) ETY-CT and (b) ETY-CTC under 980 nm light irradiation (output current = 2.0 A). The UV-vis absorption spectra of NBT are decreased at different time.

References

[1] K. Giannousi, I. Avramidis and C. Dendrinou-Samara, *RSC Adv.* 2013, **3**, 21743-21752.